Development of a Conformal Pneumatic Forebody Control For Next-Generation Fighters

Matthew J. O'Rourke*, John N. Ralston† and Stefan J. Kloc**
Bihrle Applied Research, Inc.
Hampton, VA 23666

Kevin J. Langan‡
Aeromechanics Division, Wright Laboratory
WPAFB, OH 45433

SUMMARY

A 1/9-scale model representing a realistic next-generation fighter was tested in the NASA Langley 20-Foot Vertical Spin Tunnel. Two forebodies of different cross-section were used to test seven different pneumatic devices for effectiveness in producing yawing moment. These devices included two slotted nozzles, tested to provide a baseline effectiveness level, and five conformal slot devices. Although both slotted nozzle devices produced effective levels of yawing moment, the tangential slot blowing device proved to be the most effective as well as being conformal which will help to reduce the impact of pneumatic forebody controls on low-observability. Each forebody exhibited similar levels of yawing moment for similar pneumatic devices, however, the interaction between the forebody and wing flowfields varied between the two, producing very different rolling moment interactions. Tangential slot blowing was shown to be effective on this configuration both in sideslip and rotation. In addition, a simple investigation into the transient response of the yawing moment to blowing indicated that little lag exists. A fully-functional, nonlinear, six degree-of-freedom simulation was used to model a configuration using only tangential slot blowing on the forebody for directional control and with degraded directional stability (representative of a tailless configuration). This simulation indicateded that a tailless configuration could be stabilized and execute a 45 deg/sec wind axis roll at 40° angle of attack.

---

* Engineer, Member AIAA
† Engineering Manager
** Test Engineer
‡ Aerospace Engineer WL/FIMA, Member AIAA

NOMENCLATURE

b	wing span, ft
$\bar{c}$	mean aerodynamic chord, ft
C_L	lift coefficient, $\frac{\text{Lift}}{\bar{q}S}$
C_l	rolling-moment coefficient, $\frac{\text{Rolling moment}}{\bar{q}Sb}$
C_m	pitching-moment coefficient, $\frac{\text{Pitching moment}}{\bar{q}S\bar{c}}$
C_n	yawing-moment coefficient, $\frac{\text{Yawing moment}}{\bar{q}Sb}$
C_p	pressure coefficient, $\frac{p_\infty - p_{local}}{\bar{q}}$
C_μ	blowing coefficient, $\frac{\dot{m}V_{jet}}{\bar{q}S}$
$\dot{m}$	mass flow, slug/sec
p_{WIND}	wind-axis roll rate, deg/sec
$\bar{q}$	free-stream dynamic pressure, lb/ft^2
S	wing reference area, ft^2
V	free-stream velocity, ft/sec
V_{jet}	jet exit velocity, ft/sec
α	angle of attack, deg
β	angle of sideslip, deg
θ	blowing device pointing angle, deg

Ω angular velocity about spin axis, rad/sec

$\Omega b/2V$ spin coefficient, positive for clockwise spin

INTRODUCTION

Typically, high performance aircraft are unable to achieve steady flight at high angles of attack due to loss of directional control. This loss of control is caused by the immersion of the vertical tail in the separated wing wake. This problem is further aggravated by design strategies used for next-generation fighters which typically attempt to minimize vertical control surface areas for low observability. For this reason, a great deal of research has been devoted to forebody yaw controls, specifically pneumatic forebody controls (PFC). A significantly large data base has been accumulated, beginning in the late 1970's, relating to PFC research on smooth forebodies (References 1-5). However, since the typical next-generation fighter will have a chined forebody, its forebody flowfield will differ significantly from those typical of smooth forebodies.

Over the past five years, several studies have indicated that PFC can be utilized effectively on generic configurations with chined forebodies (References 6-9). However, these studies did not explore integration of their respective pneumatic devices on realistic fighter configuration. For this reason, a study was initiated by the Air Force and conducted by Bihrle Applied Research (BAR) to determine the feasibility of several PFC concepts on an F-16 configuration modified with a chined forebody (Reference 10). Although this study was limited in scope it confirmed the results obtained on the generic models and provided an excellent starting point for this research effort. In particular, Reference 10 shows not only that the most effective PFC devices work statically at zero sideslip angle, but also that they maintain their effectiveness in both sideslip and rotation. This is not necessarily the case with PFC on smooth forebodies, which typically experience a more pronounced yaw-control effectiveness degradation in both sideslip and rotation (Reference 11). In addition, Reference 10 shows that a large rolling moment is generated along with the yawing moment, indicating that a strong interaction exists between the forebody and wing flowfields. This has not typically been seen in smooth forebody PFC research, but has been seen in the chined forebody PFC studies in References 8 and 9.

TEST EQUIPMENT

A rotary balance measures the forces and moments acting on a model while it is subjected to rotational flow conditions. Historical background for this testing is discussed in Reference 12. A sketch of the rotary balance rig in the Langley 20-Foot Vertical Spin Tunnel is shown in Figure 1. The system's rotary arm which rotates about a vertical axis at the tunnel center, is supported by a horizontal boom and is driven by a motor.

A NASA six-component strain gauge balance, affixed to the bottom of the rotary balance apparatus and mounted inside the model, is used to measure the six forces and moments acting along and about the model body axes. Controls located outside of the tunnel test section are used to activate motors on the rotary balance rig, which position the model to the desired attitude. The angle-of-attack (α) range of the rig is 0° to 90°, and the sideslip angle (β) range is ± 30°. The system is capable of rotating up to 60 rpm in either direction. A range of $\Omega B/2V$ values can be obtained by adjusting rotational speed and/or tunnel air flow velocity. Static aerodynamic forces and moments are obtained when $\Omega=0$.

A 780B Pressure Measurement System from Pressure Systems, Inc. (PSI) is used, along with eight electronic scanning pressure modules (ESP-32), to measure surface pressures. Each module contains 32 ports (for a total of 256 ports) and are rated for a maximum range of ±52 psf. Mass flow through the pneumatic devices was directly measured and controlled using a Teledyne-Hastings-Raydist mass flow controller with a range of 0-100 standard liters per minute (SLPM), or approximately 0-3.5 standard cubic feet per minute (SCFM).

MODEL DESCRIPTION

A 1/9 scale model representing a next-generation multi-role fighter, referred to herein as the X-23, was constructed by Bihrle Applied Research using fiberglass, balsa wood and plywood. The wing planform is a clipped diamond with a +40°/-40° LE/TE sweep. The wing area, S, is 4.60 ft^2 , the mean aerodynamic chord, $\bar{c}$, is 1.86 ft and the span is 3.02 ft. The empennage is comprised solely of two all-moving 'butterfly tails' which are canted outward from vertical 45°. An additional forebody was fabricated from the wing leading edge forward. This forebody employed a different cross-section and an F-16 - style canopy, and will herein be referred to as the X-16. The fuselage aft of the wing leading edge is identical to the basic F-16 fuselage. Three-dimensional sketches of the X-23 and X-16 models and their respective forebody cross-sections are shown in Figure 2.

A total of 256 pressure taps were located on the upper and lower surface of the wing (including control surfaces) and on the upper and lower side of the fuselage from the forebody apex to the trailing edge of the wing. Unfortunately, the first two rows of pressure taps had to be

removed to test the PFC devices which were implemented using removable forebody nosetips approximately 4 inches long.

A total of seven PFC devices were constructed such that they could be tested on either the X-23 or X-16 forebody. This was done by fitting all devices to a common cylindrical base (to allow each device to be pointed in any direction) of approximately 0.25" in height and 0.5" in diameter. These devices included two basic types: slotted nozzles and conformal slots. Two slotted nozzles were tested to establish baseline effectiveness, and are shown in Figure 3. They were:

1. **Jet 1**: A 3/32 in. inside diameter nozzle canted 10° and approximately 0.25 in. above the forebody surface.

2. **Jet 2**: A 1/16 in. inside diameter nozzle canted 10° and approximately 0.25 in. above the forebody surface.

Five slot configurations were tested, and are also shown in Figure 3. They were:

1. **Slot 1**: A 0.468 in. long with a 0.012 in. gap slot blowing tangential to the forebody surface.

2. **Slot 2**: A 0.16 in. long with a 0.0105 in. gap slot inclined 25° from normal to the forebody surface in the local plane normal to the forebody.

3. **Slots 3,4 and 5**: Three 0.5 in. long with a 0.012 in. gap slots inclined 30°, 45° and 65° from tangent to the forebody surface.

Each of these could be tested in two locations, 1 in. and 4 in. aft of the forebody apex, respectively, both 30° above the chine. All data presented in this paper were taken in the forward (1 in.) location. These locations were placed on both the left and right sides, making a total of four on each forebody.

TEST CONDITIONS

The tests were conducted in the NASA Langley 20-Foot Vertical Spin Tunnel at an airstream velocity of 25 ft/sec, which corresponds to a Reynolds number of approximately 300,000 based on model wing mean aerodynamic chord ($\bar{c}$). Unless otherwise noted, the various configurations were tested through an α range of 0° to 90°. The tested sideslip angles were dependent upon the configuration.

For all rotational data, the spin axis passed through the 30 $\bar{c}$ wing station. For all the rotational tests, data were obtained at each angle of attack for $\Omega b/2V$ values of 0.05, 0.1, and 0.2 in both clockwise and counter-clockwise directions, as well as for $\Omega b/2V = 0.0$ (static values).

DISCUSSION OF RESULTS

Basic Configuration Characteristics

Figures 4 shows the lift coefficient (C_L) and pitching moment coefficient (C_m), respectively, for the X-23 configuration at zero sideslip angle (β). Although the C_L and C_m data for the X-16 are not presented, they are essentially similar to those of the X-23. The angle of maximum lift occurs at about 40° α at a C_L value of approximately 1.2. The lift curve slope is shallow, and the wing stalls smoothly, which is typical of low-aspect-ratio, highly-swept wings such as the clipped diamond used on the X-23. The pitching moment data in Figure 4 show an unstable pitching moment curve up to 15° α, where it becomes neutrally stable to 20° α, maintains a stable-to-neutral slope until 60° α, where the forebody looses vortex lift and the C_m breaks sharply stable. Up to 50° α, the X-23 and X-16 show little difference in C_m. Above 60° α, the slightly larger forebody planform area of the X-23 adds slightly more nose up C_m.

Although no lateral-directional data are presented for the basic X-23, it will be discussed here briefly for completeness. Because the chines on the X-23 fix the forebody separation points, the forebody flowfield remains symmetric at all angles of attack and, therefore, produces little if any lateral or directional asymmetry at zero β. Between 10° and 20° α the X-23 is neutrally stable about the roll-axis and is slightly unstable about the yaw axis. The configuration is laterally and directionally stable at all other angles of attack. The rotational data for the basic X-23 show adequate lateral and directional damping in rotation at all angles of attack. No spin modes exist for neutral controls.

Pneumatic Forebody Control

Reference 13 indicates that a sharp included chine angle may prohibit generation of an asymmetrical forebody flowfield and thereby reduce the effectiveness of PFC. Therefore, since the X-16 has a larger included chine angle than the X-23 (i.e. the X-23 has a sharper chine), and a forebody shape essentially similar to that tested in Reference 10, it was chosen as the forebody on which to conduct the parametric investigation of the various PFC concepts. Once the most effective PFC concepts were determined, they were tested on the X-23, which is a more

realistic representation of a next-generation fighter configuration.

The parametric investigation was initiated using a slotted nozzle, a device known to be effective from many different tests (References 2,3,5,9, and 10). Once it was determined from data obtained using the slotted nozzle that PFC could be used effectively on the X-16, the investigation moved to testing the conformal slot devices which represent more realistic configurations for future fighters.

PFC On The X-16

Reference 2 explains that utilizing the slotted nozzle design provides a significant improvement in effectiveness over a simple, unslotted nozzle. Equally, if not more important is the orientation of the nozzle with respect to the forebody. For this reason, each of the seven PFC devices tested were fitted with a common, cylindrical base so that each could be interchanged into any forebody location and could be pointed in any direction in the plane tangent to the forebody.

Figure 5 shows the yawing moment coefficient, C_n, of the small slotted nozzle, tangential slot, inclined normal slot and the 65° inclined tangential slot, oriented in the most effective pointing direction, θ, for each device ($C_\mu = 0.01, \beta = 0$, right side). The small nozzle data is presented because it was slightly more effective than the large nozzle, possibly due to the sonic exit velocity of the small nozzle as compared to the subsonic exit velocity of the large nozzle. This increased effectiveness of smaller nozzles has be seen in smooth forebody research, as well (Reference 5). The 65° inclined tangential slot is presented as the most effective inclined tangential slot tested. The data in Figure 5 show clearly that the tangential slot and slotted nozzle are more effective than the 'off-surface' pneumatic devices up to maximum lift (40° α). Above maximum lift, however, the inclined slots continue to be effective up to 60° α. This indicates that if post-stall maneuvering is desired, possible slot reorientation with α may be required. However, for this study only maneuvering flight up to maximum lift and the immediate post-stall region were considered. Therefore tangential slot blowing was chosen as the pneumatic device to be used on the X-23

PFC On The X-23

Figure 6 shows C_n vs. α for the tangential slot at $C_\mu = 0.01$ and $\beta = 0$ mounted on the right side for the X-16 and on the left side for the X-23. For both forebodies, the optimum pointing angle was 135° (forward and across the forebody). The level of yawing moment with α is very similar for the X-16 and the X-23. However, the data in Figure 6 show that the rolling moment produced by tangential slot blowing at 135° is very different for the X-16 and X-23. The peak rolling moment coefficient, C_l, value of almost 0.02 on the X-16 occurs at 30° α and does not completely diminish until 50° α. This level of rolling moment is similar to that shown in References 8-10 and is attributed to an interaction between the forebody and wing flowfields.

Figure 7 shows the surface pressure contours at 35° α with tangential slot blowing on the X-16 (pilot's right side) and the X-23 (pilot's left side), at a $C\mu$=0.01 and a pointing direction of 135°. At 30° on the X-16, the low pressure region present on the left wing (right side of picture) is not present for the no blowing case. Pressure data not presented here indicate that when no blowing is present, the strong forebody vortex systems on both the left and right sides breakdown in the region of the wing leading edge, disrupting both the left and right wing flowfields simultaneously. For the tangential slot blowing case, the forebody vortex system on the left side has most likely been blown off by the tangential slot. Therefore there is no forebody vortex system on the left side to disrupt the wing flowfield. The left wing vortex persists, causing a the positive rolling moment on the X-16, shown in Figure 6, until the left wing flowfield breaks down around 40° α. For this reason, it is believed that a strong, proverse rolling moment *may* accompany PFC concepts which are effective at producing yaw if:

1. The wing flowfield is strong (i.e. a highly swept wing or a wing/lex combination)

2. The forebody vortex system in the unblown case breaks down in the region of the wing leading edge, disrupting the wing flowfield.

The X-23 pressure data in Figure 7 show no region of low pressure on the pilot's-right-side wing. This may be due to the slightly stronger and lower forebody vortex of the X-23 interacting with the wing flowfield below 35° α which disrupts the wing flowfield before it can generate a large rolling moment asymmetry. The adverse C_l on the X-23 in Figure 6 occurs over a smaller α range than the proverse C_l on the X-16, and is due mainly to the low pressure region on the pilot's left side of the forebody.

The data presented in Figures 6 and 7 clearly indicate that a strong interaction may exist between the forebody and wing flowfields based, at least in part, on the two criteria listed above. Even though the yawing moment appears unaffected, the interaction between forebody and

wing appears to be very dependent on forebody cross-section. It is the supposition of the author that variation of fineness ratio would have a similar effect on this interaction.

Yawing Moment Control

Although modulation of the yawing moment is of great importance concerning utility of PFC in an actual aircraft flight control system, the ability of PFC to maintain effectiveness in sideslip and during dynamic flight conditions is also of extreme importance. Fortunately, chine forebody configurations such as the X-23 may provide some control benefits over typical smooth forebody configurations due to the unique flowfield created by the forebody chines. Figure 8 shows the surface pressure contours for the F-15 and the X-23 at 15° and 40° α. Notice that at 15° α the surface pressures on the F-15 forebody indicate that most of its forebody is still at or only slightly higher than freestream pressure (0.0 C_p). However, the X-23 surface pressures show peak C_p levels of approximately -2.0. This difference is accentuated at 40° α which shows peak C_p values of nearly -4.0 on the X-23. Reference 13 shows that peak C_p levels on the F-15 forebody occur near 65° α at -2.3 to -2.5. This indicates a *potential* for chined configurations, specifically ones like the X-23, to generate large asymmetries in forebody sideforce, even at moderately low α. It is certain, however, that the chine-fixed flow separation will make it more difficult to create that asymmetry.

Figure 9 shows the surface pressures on the F-15 and the X-23 at 40° α undergoing a positive (clockwise) rotation of $\Omega b/2V = 0.2$. Even though a slight flow asymmetry exists for the X-23 in rotation, it is small when compared to that on the F-15. This is due to the chine-fixed forebody flow separation on the X-23. The benefit of this is that the region of low pressure remains fairly constant in rotation and sideslip in relation to the PFC device on the X-23, keeping the effectiveness achieved statically at 0° β fairly constant. Notice that the forebody flowfield on the F-15 rotates over the entire cross-section due to the model's rotation. This, in turn, moves the region of low pressure with respect to the PFC device, reducing its effectiveness. This was reported for smooth forebody PFC controls in rotation in Reference 11.

Figure 10 shows the modulation of yawing moment increment due to tangential slot blowing with C_μ levels ranging from 0.005 to 0.02. The yawing moment is easily modulated at each α up to 40°, with yawing moment increments present beyond 60° for higher blowing rates. Figure 11 shows C_n generated by tangential slot blowing at C_μ=0.01, on the left side of the X-23 at 0°, -10° and +10° β. Although some differences from the zero-sideslip effectiveness exist, tangential slot blowing in both positive and negative sideslip remains effective up to and beyond maximum lift. Figure 12 shows the effectiveness of tangential slot blowing at C_μ=0.009, on the left side of the X-23, at 35° α for both positive and negative rotation. This α is representative of the effectiveness of tangential slot blowing on the X-23 in rotation at all α. A slight reduction in the effectiveness is shown at higher rates in the propelling (negative) direction. However, a slight augmentation of the effectiveness occurs in the direction used to arrest a maneuver or departure.

Now that controllability, effectiveness in sideslip and effectiveness in rotation of PFC on the X-23 has been demonstrated, it is necessary to determine if any lags exist between blowing at the forebody and the generation of yawing moment. Unfortunately, this is a difficult effect to quantify due to unknown levels of lag in the actuation system and in the pressure build-up in the supply line. In an attempt to bypass these lag sources, the line pressure was sensed directly (approximately 1") upstream of the slot exit. The line pressure was sensed using a Kulite pressure transducer capable of measuring time-dependent variations in pressure in the microsecond range. The resulting time history, shown in Figure 13, shows no perceivable lag between the yawing moment response and the input blowing. Similar data (not shown) indicate a similar responsiveness of PFC in rotation, as well. Although not all-conclusive, this simple test provides a strong indication that, with careful design, PFC can be implemented without introducing appreciable lags in response.

Six-Degree-Of-Freedom, Nonlinear Simulation

A brief description of the control system and the database is followed by two simulated flight excursions with a "Tailless X-23" with and without PFC. Basic F-16A weights and inertias are used for the X-23 in the simulation runs.

Database and Control System

The control system was not intended to be robust or satisfy any handling qualities criteria. It was intended, however, to stabilize the X-23 up to and beyond maximum lift and coordinate wind-axis roll maneuvers. To this end a simple alpha-command system with alpha-rate feedback was used for longitudinal control and stability augmentation. Laterally, the ailerons were commanded directly by the lateral stick, with stabilization provided by roll-rate feedback. Finally, β was minimized using sideslip and sideslip-rate feedback as well as an aileron-PFC interconnect to drive the PFC for the Tailless X-23 runs. A 0.10 sec, first-order lag was placed on the PFC response

The wind tunnel data were combined for each moment and force to arrive at the total coefficient for each. Each total coefficient is a sum of individual coefficient increments which attempt to model all dependencies on α, β, rotation, control deflections and their mutual interactions. These total coefficients are substituted into the nonlinear equations of motion which are integrated using a fourth-order Runge-Kutta integration scheme. Using the Bihrle Applied Research simulation environment, ***D-Six***, the control system gains were entered as tables, and modified until desirable flight dynamic characteristics were achieved.

For both PFC on and off simulation runs, a "loaded roll reversal" maneuver was used. This maneuver is initiated at 5° α and rolls 90° as to the left, followed by a 6-g pull to approximately 40° α. At approximately 40° α and 5 g's a maximum-roll-rate wind axis roll is initiated to the right. This roll is carried out for 270° of bank, and wings are leveled when heading is reversed (180°). The throttle position is set at maximum thrust for the maneuver.

Tailless X-23 Simulation with PFC

Since the differential tails on the X-23 were more than adequate to provide controlled, maneuvering flight up to maximum lift, it was decided that the only effective test of PFC as a control would be on the X-23 with no other directional control effectors. This was achieved by eliminating the effect of differential tails in the database, and significantly degrading the directional stability, representative of a configuration with horizontal tails only. However, this degradation in directional stability was only applied above 10° α due to limited PFC control effectiveness at low α. It is assumed that split-flap or similar devices on the wing trailing edges can augment PFC low-α stability and control, if necessary.

Figure 14 shows the time histories generated during the loaded roll maneuver with PFC turned on. The β hold is fairly good throughout the maneuver, never increasing beyond approximately 3°. Certainly, the control system could be optimized more completely to minimize the oscillation, but the wind axis roll rate of approximately 45° deg/sec at 40° α shows excellent high-α maneuverability compared to the current generation of fighters.

Tailless X-23 Simulation without PFC

Figure 15 shows the time history generated using the loaded roll maneuver stick and throttle inputs with PFC turned off (i.e. without any directional control). During the first roll segment at 5° α, a β excursion to 5° is encountered. Since the configuration is directionally stable at this angle of attack, β returns to zero. However, after the pull to 40° α, the directional instability causes positive β to increase rapidly when the right roll input is made. Therefore, instead of rolling to the right, the positive β causes the aircraft to roll off to the left. The negative (left) wind axis roll rate and positive β increase until the directional damping stabilizes the aircraft in a spin-like condition that oscillates in pitch and yaw. When the angle of attack is reduced, the wind axis roll rate decreases and the aircraft becomes more stable, albeit at a moderate level of sideslip.

These brief simulation examples show that PFC can be used to stabilize an unstable aircraft. In addition, PFC can provide enough control power to perform aggressive lateral-directional maneuvers at high angles of attack.

CONCLUSIONS

A conformal pneumatic control device employing tangential slot blowing was developed which provides effective levels of yaw control on a realistic configuration representative of future fighters. This device was the result of a parametric investigation examining forebody cross-section, device location, device orientation, and different slot and jet geometries. The optimum configuration was determined to be tangential slot blowing located at the near the apex of the forebody blowing forward and inboard, across the nose. This configuration was tested at different blowing levels, sideslip angles and rotation rates. In all cases the yawing moment increment was found to be robust and controllable. A simple test to determine the transient yawing moment response, indicated little or no control lags. When the wind tunnel database and a simple control system were used in a nonlinear six-degree-of-freedom simulation, it was found that PFC can be used to provide controlled, highly-maneuverable flight up to maximum lift.

ACKNOWLEDGEMENTS

The research presented in this paper is the result of an Air Force Phase II SBIR study. The authors would like to thank Mr. Russell Osborn of the Aeromechanics Division of Wright Laboratory for his guidance and support.

REFERENCES

1. Skow, A. , Moore, W., Lorincz, D.: "Forebody Blowing - A Novel Concept to Enhance the Departure/Spin Recovery Characteristics of Fighter Aircraft," AGARD CP-262, May 1979.

2. Guyton, R. and Maerki, G.: "X-29 Forebody Jet Blowing," AIAA 92-0017, January 1992.

3. Lemay, S. , Sewall, W. and Henderson, J.: "Forebody Vortex Flow Control on the F-16C Using Tangential Slot and Jet Nozzle Blowing," AIAA-92-0019, January 1992.

4. Lanser, W.R.: "Forebody Flow Control on a Full-Scale F/A-18 Aircraft," AIAA-92-2674, June 1992.

5. Iwanski, K., O'Rourke, M.: "F-15 Forebody Vortex Flow Control Using Jet Nozzle Blowing," AIAA-95-1800, June, 1995.

6. Boalby, R., Ely, W., Hahne, D.: "High Angle of Attack Stability and Control Concepts for Supercruise Fighters," NASA CP-3149 Part II, October 1990.

7. Rao, D., Sharma, G.: "Mechanical and Pneumatic Concepts for Side-Force Control on a Forebody of Diamond Cross-Section at High Angles of Attack," WL-TR-92-3120, November 1992.

8. O'Rourke, M.: "Experimental Investigation of Slot Blowing for Yaw Control on a Generic Fighter Configuration with a Chined Forebody," AIAA-95-1798, June 1995.

9. O'Rourke, M., Sedor, J.: "Forebody-Mounted Jet Nozzles for Yaw Control on a Generic Fighter Configuration with a Chined Forebody," AIAA-95-3490, August 1995.

10. Ralston, J., Avent, J., Dickes, E.: "A Feasability Study of Vortex Control on a Chined Forebody," WL-TR-93-3027, January 1993.

11. Simon, J., LeMay, S., Brandon, J.: "Results of Exploratory Wind Tunnel Tests of F-16/VISTA Forebody Vortex Control Devices," WL-TR-93-3013, January 1993.

12. W. Bihrle, Jr. and Barnhart, "Spin Prediction Techniques," *Journal of Aircraft*, Volume 20, Number 2, February 1983.

13. Kegelman, J., Roos, F.: "Influence of Forebody Cross-Section Shape on Vortex Flowfield Structure at High Alpha," AIAA-91-3250, September 1991.

14. Kay, J., Ralston, J.: "F-15E High Angle of Attack Study, Including Data, Analysis, Aerodynamic Math Modeling and Simulation," Bihrle Applied Research, Inc., BAR 95-2, March 1995.

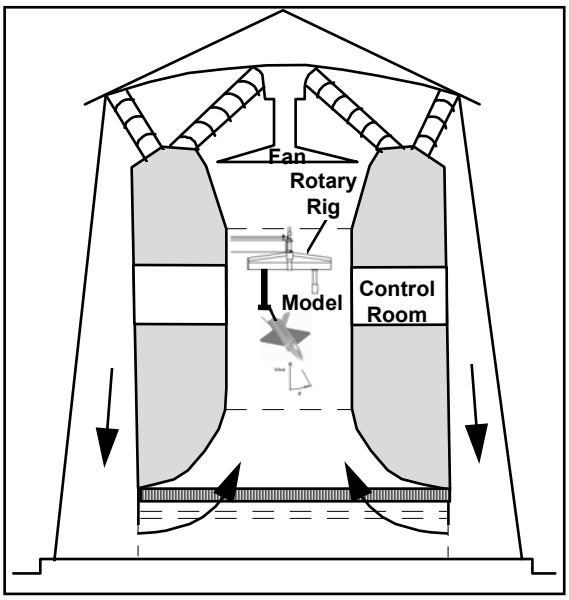

Figure 1.- Sketch of the X-23 mounted on the rotary balance rig in the NASA Langley 20-Foot Vertical Tunnel.

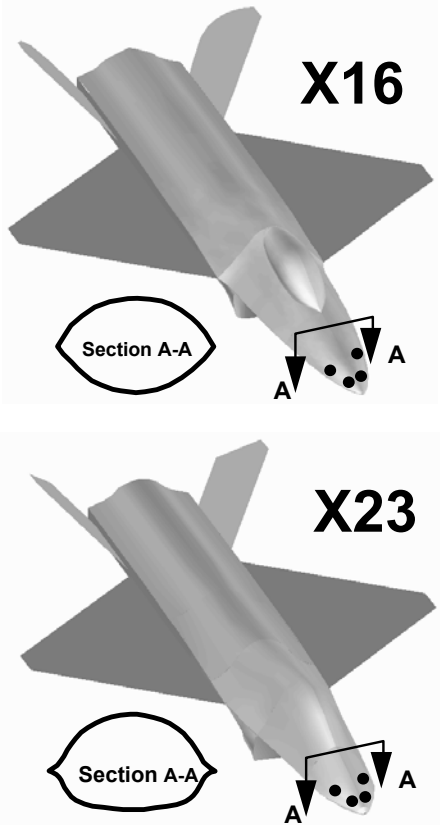

Figure 2.- Sketches of the X-16 and X-23 configurations.

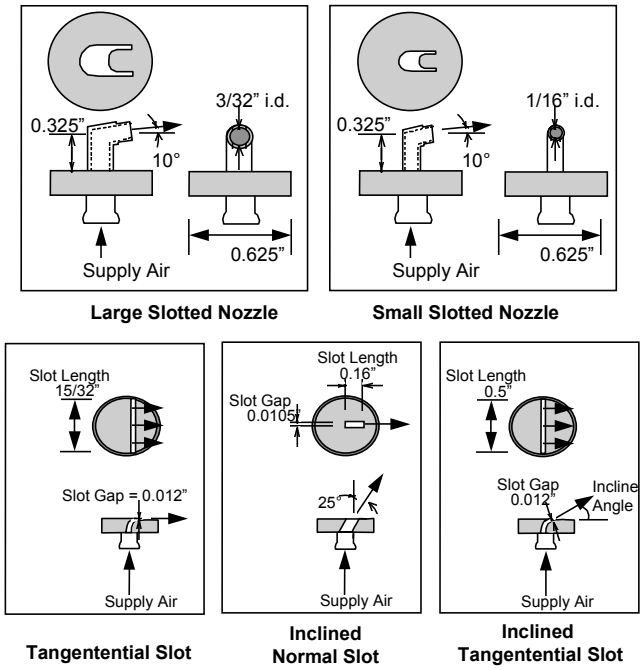

Figure 3.- Sketches of the various pneumatic devices used in this investigation.

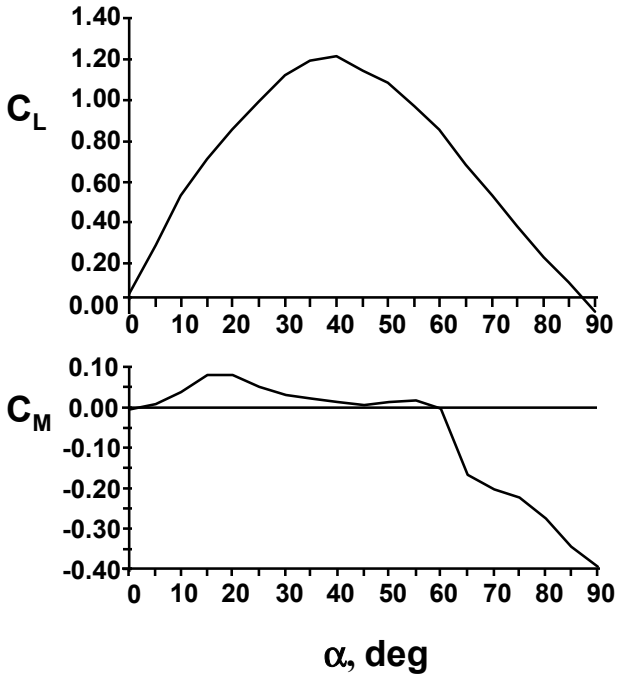

Figure 4.- Basic longitudinal aerodynamic characteristics of the X-23.

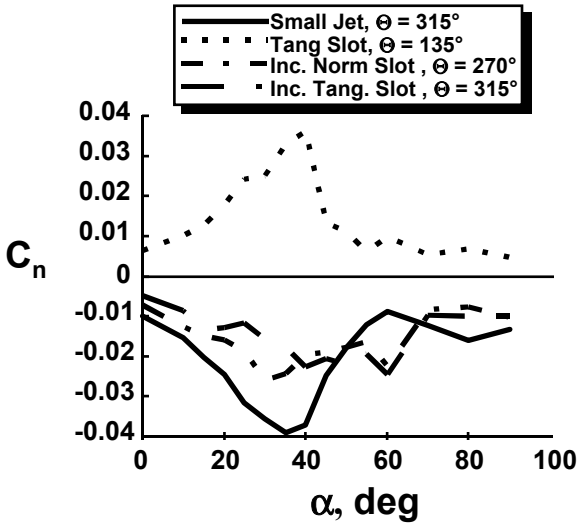

Figure 5.- Effectiveness of the various pneumatic devices in the optimum orientation.

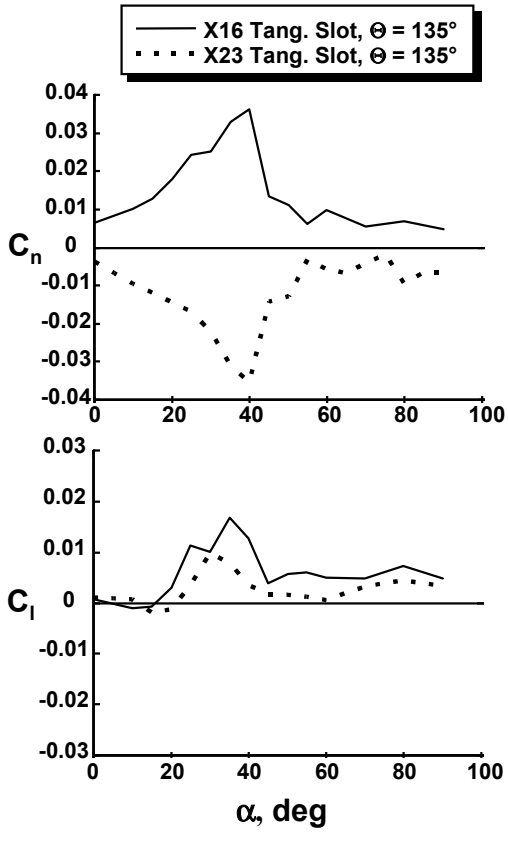

Figure 6.- Comparison of tangential slot blowing effectiveness on the X-16 and X-23.

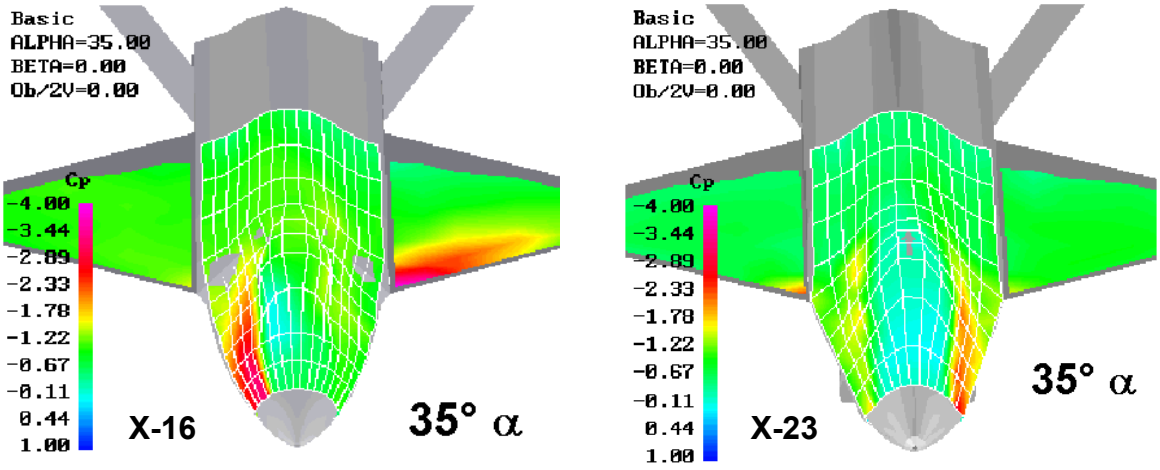

Figure 7.- Surface pressure comparison between the X-16 and X-23 with tangential slot blowing (C_μ=0.01) at 35° α.

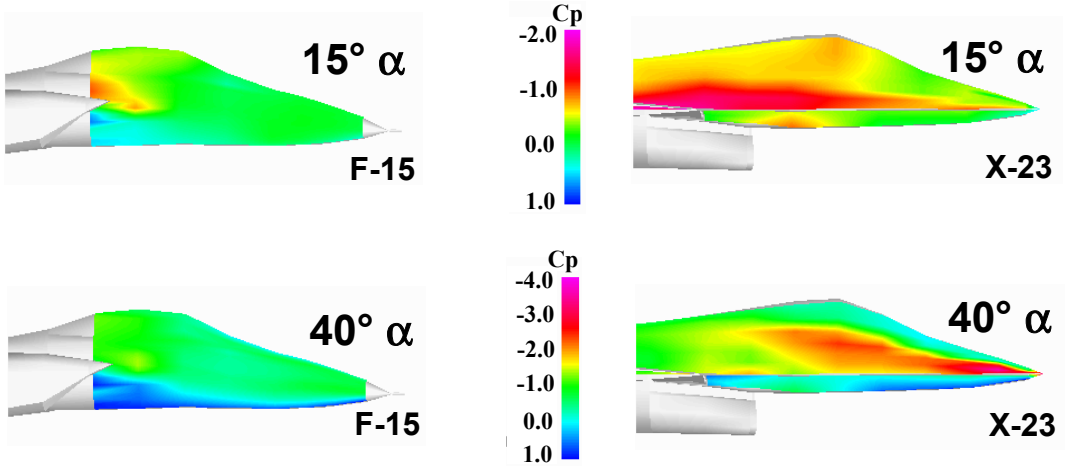

Figure 8.- Static surface pressure comparison between the F-15 and X-23 at 15° and 40° α.

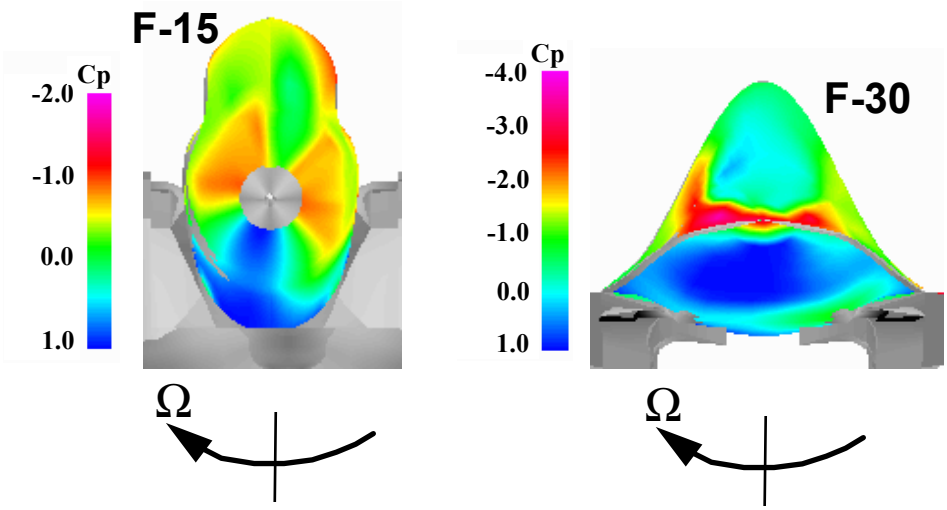

Figure 9.- Rotational surface pressure comparison between the F-15 and X-23 at 40° α.

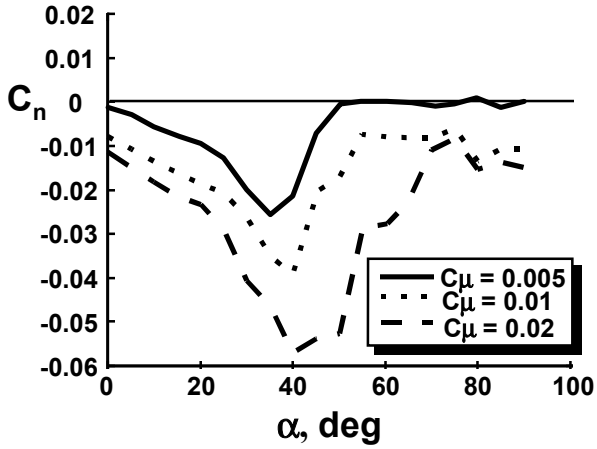

Figure 10.- Modulation of yawing moment using tangential slot blowing on the X-23 (left side).

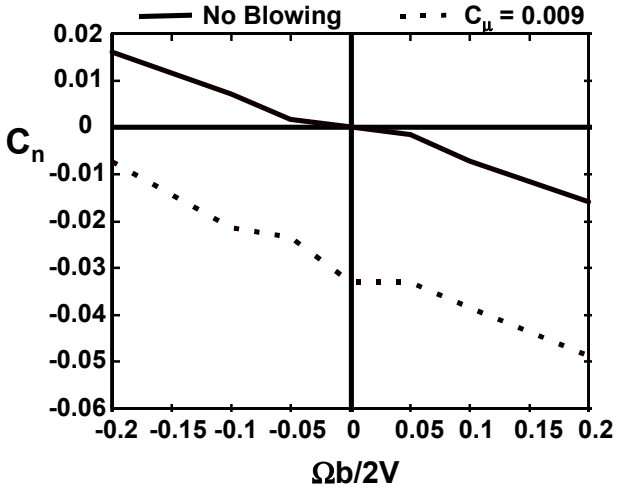

Figure 12.- Effectiveness of tangential slot blowing on the X-23 (left side) in rotation at 35° α.

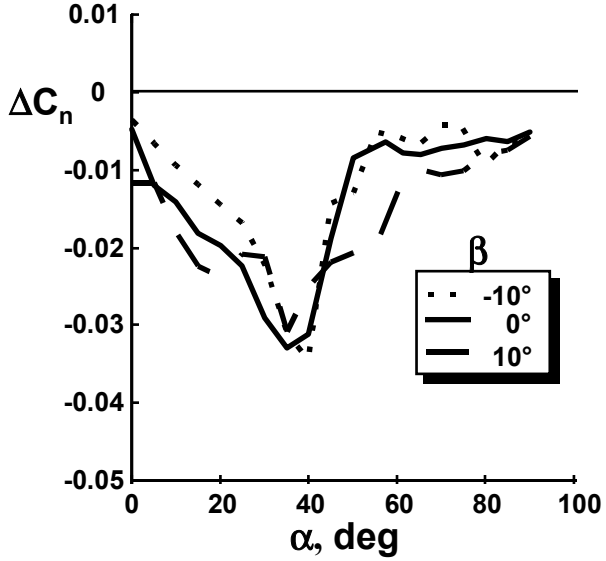

Figure 11.- Effectiveness of tangential slot blowing on the X-23 (left side) in sideslip.

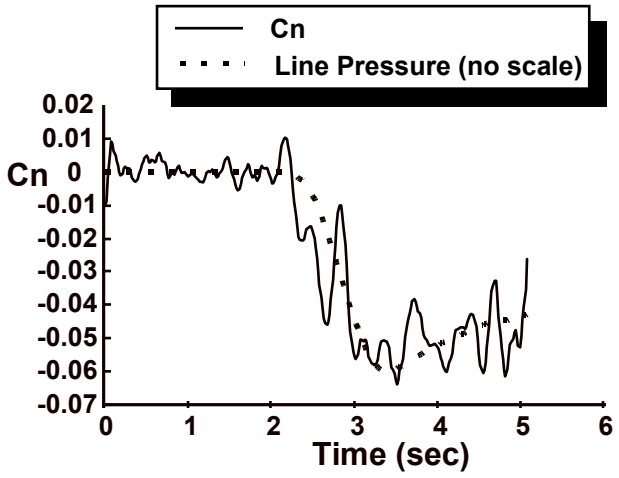

Figure 13.- Transient response of yawing moment to tangential slot blowing on the X-23 (left side).

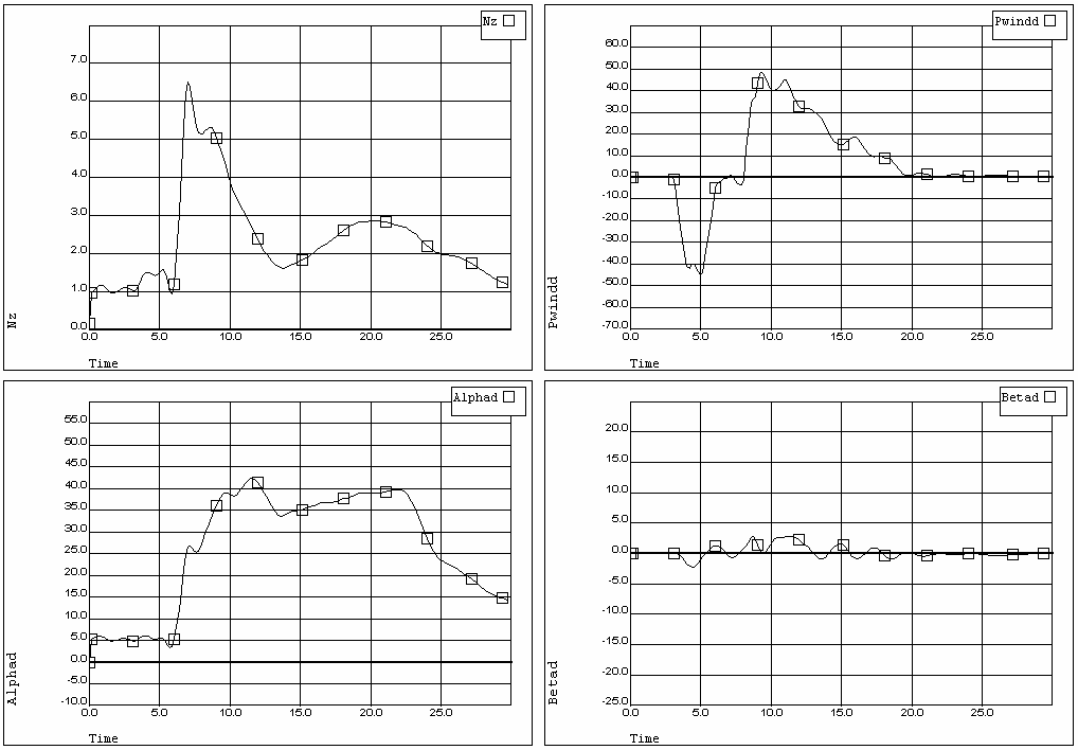

Figure 14.- Time history of flight simulation using ‘loaded roll reversal’ maneuver, PFC on.

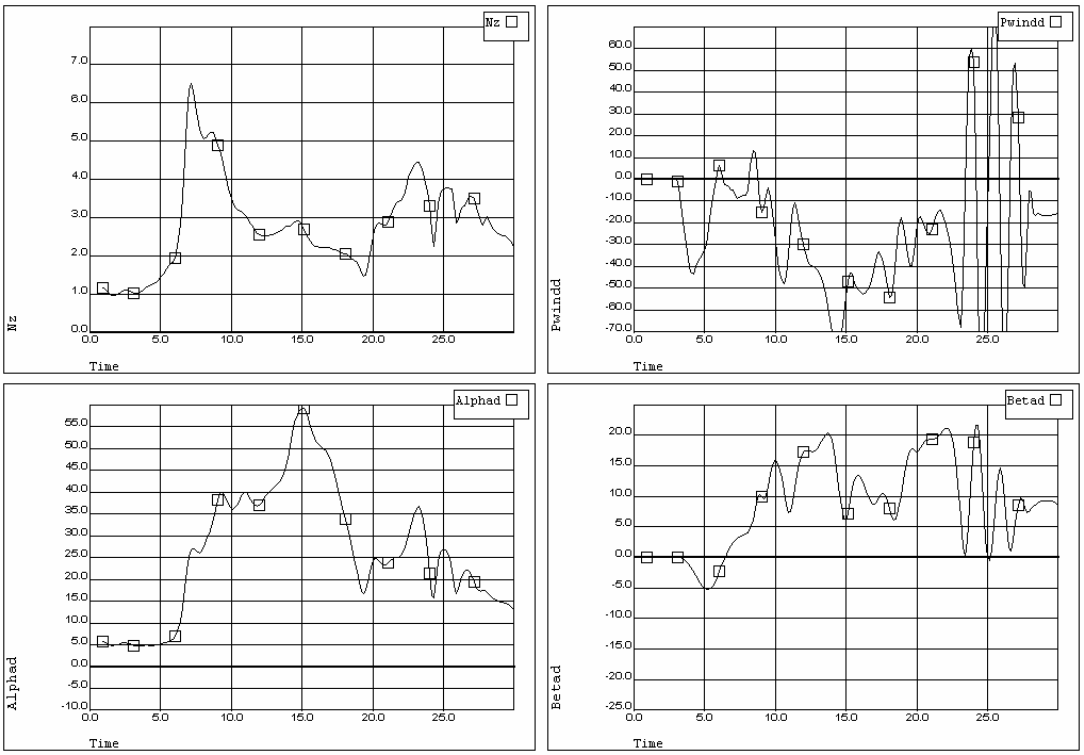

Figure 15- Time history of flight simulation using ‘loaded roll reversal’ stick inputs, PFC off.